Honorable Mention Poster Award

Frequency Diversity in Breast Ultrasound Tomography

F. Simonetti [a,b], L. Huang [b], N. Duric [c]

[a]Department of Mechanical Engineering, Imperial College, SW7 2AZ, London, UK;
[b]MS D443, Los Alamos National Laboratory, Los Alamos, NM 87545, USA;
[c]Karmanos Cancer Institute, Wayne State University, 4100 John R, Detroit, Michigan 48201, USA

ABSTRACT

The development of ultrasound tomography for the detection of breast cancer could have a major impact on the effectiveness of current diagnostic tools. Here, the potential of ultrasound tomography is investigated by means of a new generation of toroidal ultrasound arrays that can measure both the signals reflected and transmitted through human breast, simultaneously. Experiments performed on phantoms and human breast *in vivo* are used to compare continuous wave (CW) insonification versus wideband (WB) excitation. It is shown that while transmission diffraction tomography has little benefit from WB excitation, reflection tomography is greatly improved due to the low signal-to-noise ratio of reflection measurements.

Keywords: Arrays, Breast, Frequency, Speckle, Ultrasound Tomography

1. INTRODUCTION

Since the 1970s, researchers have been exploring the potential of ultrasound sonography[1,2] and tomography[3] for the detection of breast cancer. In fact, ultrasound is intrinsically safe compared to the gold standard of X-ray mammography, it can detect some cancers that are invisible on mammograms and could lead to earlier diagnosis.[4] In addition, ultrasound technology is inexpensive compared to X-ray or MRI, thus offering the potential for the development of a dense network of screening centers that could deliver diagnostic capabilities to the bulk of the population at risk.

Recent progress in solid state electronics and increased computational power have reinvigorated interest in this area and much effort is now being devoted to the development of a new generation of ultrasound scanners that employ a toroidal array of sensors.[5–8] The array is immersed in a water bath that provides the background medium and is used to insonify the breast, suspended within it, from all possible angles in the plane of the array. For each insonification the ultrasonic field scattered by the breast is detected by all the array sensors in parallel as depicted in Fig. 1(a). This full view configuration can be used to perform transmission measurements through the breast in conjunction with the more conventional backscattering measurements obtained with linear array probes. The combination of backscattering and transmission measurements can then be used to extract accurate information about the speed of sound, attenuation and density distribution within the breast. Backscattering measurements are used to reproduce compound beamforming[3] synthetically and lead to the so-called reflection image (RI). A subset of the array sensors is used to create a virtual aperture which produces different images of the breast that are combined together as the aperture revolves around the breast.[8] On the other hand, different imaging algorithms have been proposed to reconstruct speed of sound maps from transmission measurements. The computerized ultrasound tomography (CUT) approach is based on the ray approximation of geometrical optics. Transmission measurements are used to estimate the arrival time of the ballistic transmission through the breast which is subsequently used to reconstruct the speed of sound map via the Radon transform.[9] Promising results for human breast *in vivo* have been reported in the early work by Carson et al.[3] that used transducers mechanically scanned around the breast, and more recently by Duric et al.[8] with a 256 sensor toroidal array. However, the ray approximation is known to cause resolution degradation and image artifacts due to its inability to account for diffraction.[10] Therefore, it is possible that more sophisticated methods such as diffraction tomography[11,12] could improve the image quality. In this context, some initial results have been reported by Andrè et al..[5]

Medical Imaging 2008: Physics of Medical Imaging, edited by Jiang Hsieh, Ehsan Samei,
Proc. of SPIE Vol. 6913, 69134E, (2008) · 1605-7422/08/$18 · doi: 10.1117/12.772791

While CUT requires the use of wideband (WB) insonification to time the journey of ultrasound through the breast, RI and diffraction tomography (DT) can also be performed with continuous wave (CW) excitation. This is because both RI and DT can be seen as interferometric techniques that exploit spatial interference caused by waves transmitted and detected by transducers at different points in space. Therefore, the question arises whether the application of WB insonification in RI and DT leads to better image quality than CW excitation.

Although CW insonification can be related to the WB one by the Fourier transform, the analysis is complicated by a number of scattering phenomena that take place within complex media such as human breast. For example, one of the problems encountered in conventional sonography is the characteristic granular appearance of sonograms caused by the speckle phenomenon. This is a result of complex interference patterns that are due to the coherent nature of ultrasound[13] and can affect RI and DT. Although speckle contrast is used to separate different features within an image, the appearance of speckle can also mask small abnormalities. Therefore, it is interesting to investigate to which extent the frequency content of the insonification affects the presence of the speckle*. Moreover, for complex random media it has been suggested that WB excitation could lead to superior image quality than CW insonification since a WB signal propagating through such a medium would be affected more by the global structure of the medium than the local, random inhomogeneities.[14]

This paper presents a comparison between CW and WB reconstructions obtained from measurements performed on phantoms and a human breast *in vivo*. The analysis is aimed at assessing the role of WB excitation on different coherent imaging methods i. e. RI and DT. Section 2 reviews the main aspects of the theory of coherent imaging. Section 3 introduces the concept of incoherence in optical imaging and explains the role of WB excitation in ultrasound imaging. Section 4 presents three sets of experiments performed with a gel phantom, a breast phantom and a human breast *in vivo*.

2. COHERENT IMAGING METHODS

Here, DT is considered first. The aim of DT is to reconstruct the spatial distribution of a target material property, defined by the object function † $\mathrm{O}(\mathbf{r})$, from the perturbation induced by the object's structure on the free propagation of ultrasound. Central to this is the existence of a one-to-one mapping between the perturbation, p, and the spatial Fourier transform of the object function, O, which defines the so-called K-space,

$$p \longleftrightarrow O. \tag{1}$$

The definition of the perturbation in eq. (1) depends on the model used to describe the interaction between the incident wave and the probed object. To illustrate this, let us consider the two-dimensional scattering problem depicted in Fig. 1(a) whereby a monochromatic (CW) plane wave propagating in the direction $\mathbf{r}_0$ is incident on an object of support D. Assuming that the scattering problem can be expressed by a scalar potential, the field detected by an array sensor placed in the far field at position $\mathbf{r}$, $\psi(\mathbf{r}, k\hat{\mathbf{r}}_0)$, is given by

$$\lim_{r\to\infty} \psi(\mathbf{r}, k\hat{\mathbf{r}}_0) = \exp\left(ik\hat{\mathbf{r}}_0 \cdot \mathbf{r}\right) + f(k\hat{\mathbf{r}}, k\hat{\mathbf{r}}_0)\frac{\exp\left(ikr\right)}{\sqrt{r}}, \tag{2}$$

where the first term of the right hand side is the incident plane wave, which propagates with wavelength λ ($k = 2\pi/\lambda$), and $f(k\hat{\mathbf{r}}, k\hat{\mathbf{r}}_0)$ is the scattering amplitude defined as

$$f(k\hat{\mathbf{r}}, k\hat{\mathbf{r}}_0) = \Pi \int_D d^2r' \exp(-ik\hat{\mathbf{r}} \cdot \mathbf{r}')O(\mathbf{r}')\psi(\mathbf{r}', k\hat{\mathbf{r}}_0), \tag{3}$$

with

$$\Pi = \frac{\exp(i\pi/4)}{\sqrt{8\pi k}}. \tag{4}$$

*The same phenomenon is not observed in CUT that leads to speckle-free images[3, 8]

†The object function is relate to the index of refraction map, $n(\mathbf{r})$, via the relationship $O(\mathbf{r}) = k^2[n(\mathbf{r})^2 - 1]$

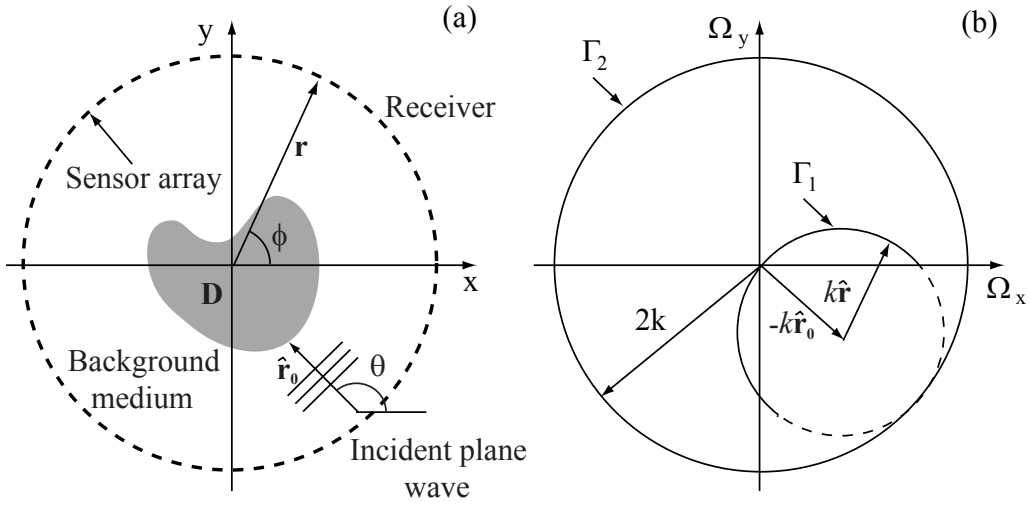

Figure 1. (a) Diagram of a toroidal array used in ultrasound tomography. (b) Two dimensional K-space showing how the scattered field measured in the direction $\hat{\mathbf{r}}$ and due to an incident plane wave from direction $\hat{\mathbf{r}}_0$ maps onto the point $\Omega = 2\pi/\lambda(\hat{\mathbf{r}}_0 - \hat{\mathbf{r}})$ of the K-space.

It can be shown that under the Born approximation, the perturbation p in eq. (1) coincides with the scattering amplitude[15]

$$p(k\hat{\mathbf{r}}, k\hat{\mathbf{r}}_0) = f(k\hat{\mathbf{r}}, k\hat{\mathbf{r}}_0) = \Pi O[k(\hat{\mathbf{r}} - \hat{\mathbf{r}}_0)]. \tag{5}$$

This relationship links the measurements to the Fourier transform of the object function, $O(\Omega)$, directly. In fact, the scattering amplitude can be measured experimentally with a toroidal array of transreceivers, by transmitting with each sensor sequentially and detecting the total field with all the sensors in parallel. The scattered field is then obtained by subtracting the incident field, measured before placing the object within the array, from the total field. The diagram in Fig. 1 shows how a particular transmit and receive pair maps onto a point of the K-space. In particular, for a given transmitter position defined by $\hat{\mathbf{r}}_0$, the measurements map onto the circle Γ_1 as the receiver direction, $\hat{\mathbf{r}}$, spans the entire array. This is known as the Ewald circle. The solid part of the circle corresponds to the so-called transmission measurements (the angle between $\hat{\mathbf{r}}$ and $\hat{\mathbf{r}}_0$ is less than $\pi/2$) whereas, the dashed part corresponds to the backscattering measurements. As the position of the transmitter revolves around the object, the Ewald circle sweeps a disk of the K-space with radius $2k$ known as the Ewald Limiting Disk (ELD) and labeled as Γ_2 in Fig. 1(b).

From the knowledge of $O(\Omega)$ within the ELD, $O(\mathbf{r})$ can be reconstructed by assuming that $O(\Omega)$ vanishes outside the ELD and performing the inverse Fourier transform. This leads to a low pass filtered image of the object function, I_{DT}, which in the K-space is given by

$$I_{DT}(\Omega) = O(\Omega) H_{DT}(\Omega), \tag{6}$$

with

$$H_{DT}(\Omega) = \begin{cases} 1 & |\Omega| < 2k \\ 0 & |\Omega| > 2k. \end{cases} \tag{7}$$

Physically this means that only the characteristics of the object that vary on a spatial scale longer than $\lambda/2$ can be reconstructed leading to the classical diffraction limit.

In transmission diffraction tomography (TDT), the object function is reconstructed from only the transmission measurements. Therefore, as the transmitter revolves around the object, the half solid circle in Fig. 1(b)

describes a disk of radius $\sqrt{2}k$ centered at the origin and contained within the ELD. In other words, transmission tomography provides a low pass filtered image with cutoff $\sqrt{2}k$ rather than $2k$. A similar argument shows that reflection diffraction tomography (RDT) provides a band pass filtered image of the object with cutoffs at $\sqrt{2}k$ and $2k$. This analysis suggests that RDT complements TDT by reconstructing the spatial frequencies between $\sqrt{2}k$ and $2k$.

These theoretical results can be used to characterize RI which is based on beamforming. In fact there exists a linear mapping that transforms RDT in RI as shown in.[16] In the spatial frequency domain, the mapping corresponds to a linear filter that attenuates the spatial frequencies of the object in the order of λ and amplifies those tending to $\lambda/2$.

3. COHERENCE VERSUS INCOHERENCE

The analysis carried out in the previous section has considered CW excitation only; therefore, it refers to perfectly coherent case. In particular, all the methods in Sec. 2 provide an image of the actual object function, which is the convolution of the object function with the point spread function (PSF), h,

$$I(\mathbf{r},\omega) = \int_D d^2r' h(\mathbf{r}-\mathbf{r}',\omega) O(\mathbf{r}'), \tag{8}$$

where the PSF is a function of frequency and depends on the type of imaging method. When the object contains inhomogeneities with a characteristic size smaller or in the same scale as the size of the PSF main lobe and randomly distributed in space, the convolution in eq. (8) results in the speckle phenomenon.

In optics it is well known that speckle is eliminated by WB illumination. In fact, optical detectors average the intensity of light over a time interval that is much longer than the characteristic period of the wavepackets. This means that in optics a WB image is given by the incoherent superposition of all the monochromatic images, $I(\mathbf{r},\omega)$, that could be reconstructed if it was possible to separate the different frequency components of the illumination

$$I_{incho}(\mathbf{r}) = \int_\infty^\infty d\omega |I(\mathbf{r},\omega)|^2. \tag{9}$$

On the other hand, ultrasonic sensors lead to an almost instantaneous measurement of the wave field, thus allowing the harmonics contained in the insonification to be separated. As a result, RI with WB excitation is still a coherent process. In fact, the wideband version of eq. (8) becomes

$$I_{WB}(\mathbf{r}) = \left| \int_\infty^\infty d\omega I(\mathbf{r},\omega) \right|^2, \tag{10}$$

where different monochromatic images are added coherently. The same argument applies to TDT and RDT. Moreover, for this reason speckle is present in sonography despite the fact that it uses broadband excitation.

4. EXPERIMENTS

Three sets of experiments were performed with a 256 element ultrasonic array developed at Karmanos Cancer Institute.[8,17] The tests were carried out with a gel phantom, a breast phantom and a human breast *in vivo* using the setup depicted in the diagram of Fig. 1(a). Both the array and the specimen where immersed in a water bath.

4.1. Gel phantom

This specimen consisted of a water based gel cylinder of 35mm diameter with a hole of 5mm diameter in the center. The hole was filled with cold water so as to produce an inclusion with a low speed of sound. The temperature of the water bath was 25.7C^o. Figure 2 shows the modulus of the scattering amplitude at 1.2MHz as a function of the insonification direction Θ and the scattering angle Φ. The color scale is in dB and represents

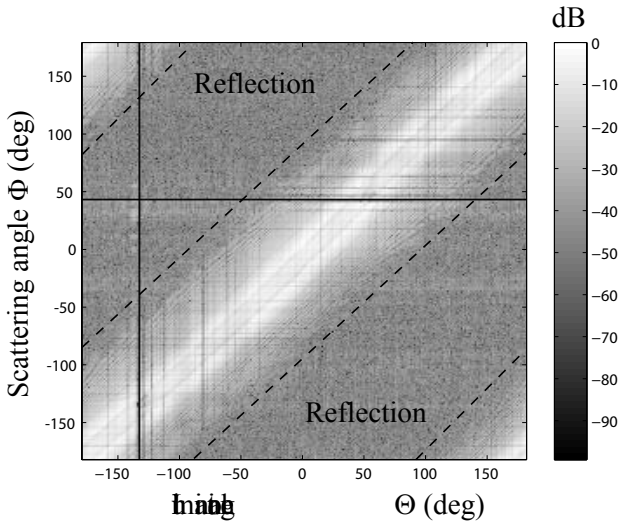

Figure 2. Modulus of the scattering amplitude at 1.2MHz as a function of the illumination angle Θ and the scattering angle Φ.

the modulus normalized with respect to the largest measurement. The bright central diagonal that extends towards the two dashed lines corresponds to the transmission measurements along with the two triangular bands on the top left and bottom right corners. The backscattering measurements correspond to the two remaining reflection bands. Details about the calculation of the scattering amplitude are given in.[17]

Figure 3(a) is the CW DT image of the phantom at 1.2MHz obtained using both the reflection and transmis-

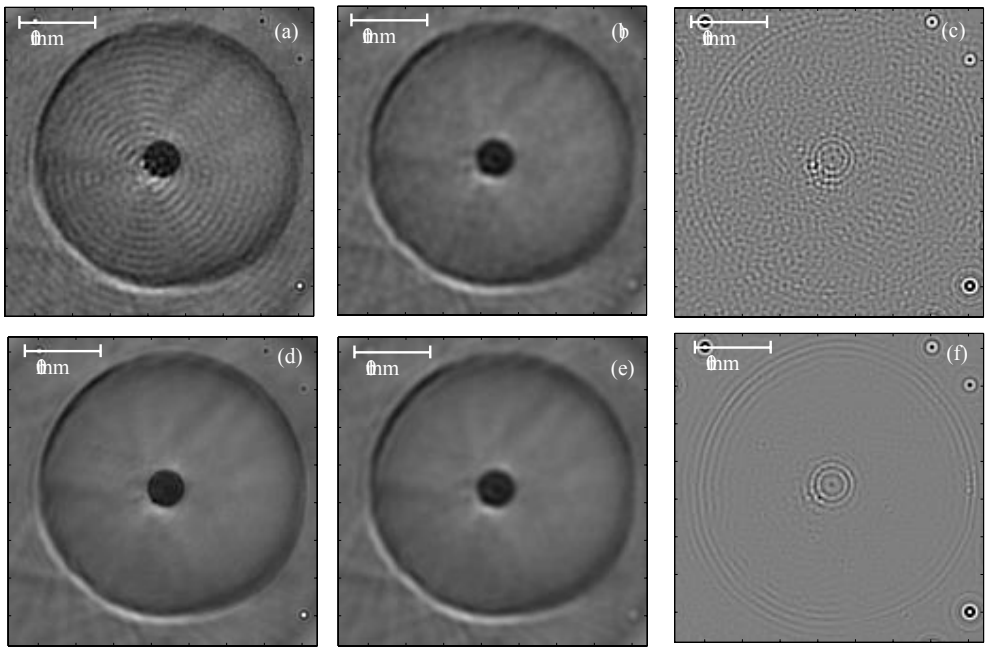

Figure 3. (a)-(c) CW images of the phantom at 1.2MHz. (d)-(f) broadband (1.1-1.3MHz) images. (a) and (d) diffraction tomography; (b) and (e) transmission tomography; (c) and (f) reflection tomography.

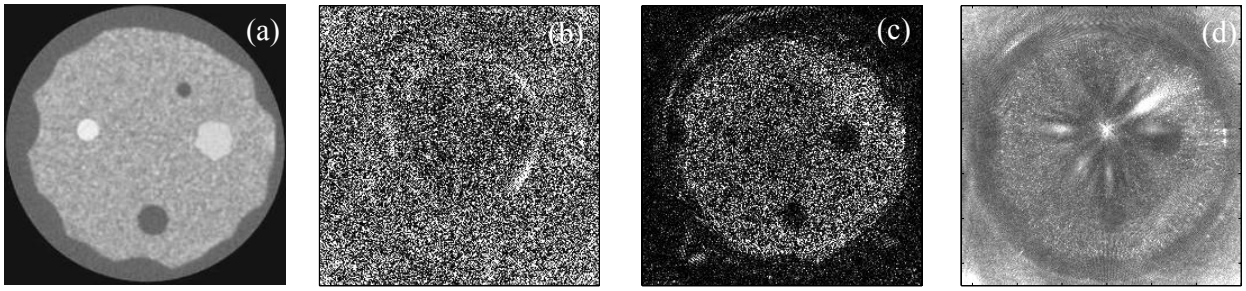

Figure 4. (a) X-ray CT image of the phantom; (b) CW RI at 1.2MHz; (c) coherent RI with 600kHz bandwidth; (d) incoherent RI with the same bandwidth as in (c).

sion data in Fig. 2. Details about the algorithm used to produce the image can be found in.[16] Next, Figs. 3(b) and (c) are the images obtained with TDT and RDT. The TDT image reproduces all the features of the phantom and is similar to the image in Fig. 3(a). In contrast, the RDT image provides a low resolution and noisy reconstruction; the boundaries of the phantom are barely visible. Figures 3(d)-(f) show the WB versions of the images in Figs. 3(a)-(c) reconstructed over the bandwidth 1.1-1.3MHz. While the TDT image does not benefit from the broadband excitation significantly [Figs. 3(b) and (e)], the broadband RDT contains a lower level of noise than the CW image [Figs. 3(c) and (f)].

It could appear that the granularity of the image in Fig. 3(c) is due to the speckle phenomenon. However, this is not true as the phantom did not contain inhomogeneities. Instead, the granularity is due to the poor signal-to-noise-ratio (SNR) of the backscattering measurements as it can be deduced from Fig. 2. This effect disappears in Fig. 3(b) thanks to the higher SNR of the transmission measurements. For the simple phantom considered in these experiments, it can be concluded that frequency diversity only improves RDT when the SNR is low and has minimal effect on TDT.

4.2. Breast phantom

In order to study the speckle phenomenon, a second set of experiments was performed on a complex breast phantom whose X-ray CT image is shown in Fig. 4(a). The phantom consists of several materials mimicking a subcutaneous fat layer that embeds an irregular glandular tissue containing four different, 3-D inclusions corresponding to two tumors and two fat spheres.[8] The glandular material contains a fine powder which reproduces the fine structure of the breast and leads to speckle in a conventional sonogram. Fig. 4(b) is a CW RI at 1.2MHz. As in the case of the gel phantom, the image is dominated by noise due to the poor SNR of the backscattered signals and is not possible to distinguish any of the structures in the phatom. Next, Fig. 4(c) is a coherent WB image over a bandwidth of 600kHz obtained with eq. (10). Thanks to the WB excitation, random noise is averaged out and an image of the glandular tissue and two of the masses is obtained. Speckle is clearly present and its contrast leads to the identification of the contours of the glandular region and the two masses. Finally Fig. 4(d) is the incoherent version of Fig. 4(c) obtained by means of eq. (9). As expected, the speckle contrast in Fig. 4(d) is lower than in Fig. 4(c). Therefore, while frequency diversity does not reduce speckle content in WB coherent imaging, incoherence has a beneficial effect. However, while coherent WB imaging tends to average out random noise, this is amplified in incoherent imaging as shown by the large bright artifacts in Fig. 4(c). Transmission measurements, not shown here for brevity, reproduce the same results observed for the gel phantom.

4.3. Human breast *in vivo*

This set of experiments was carried out with a patient lying on a bed with her breast suspended within the array through a circular aperture in the bed.[8] As in the case of the two phantoms, the reflection measurements are weaker than the transmission ones.

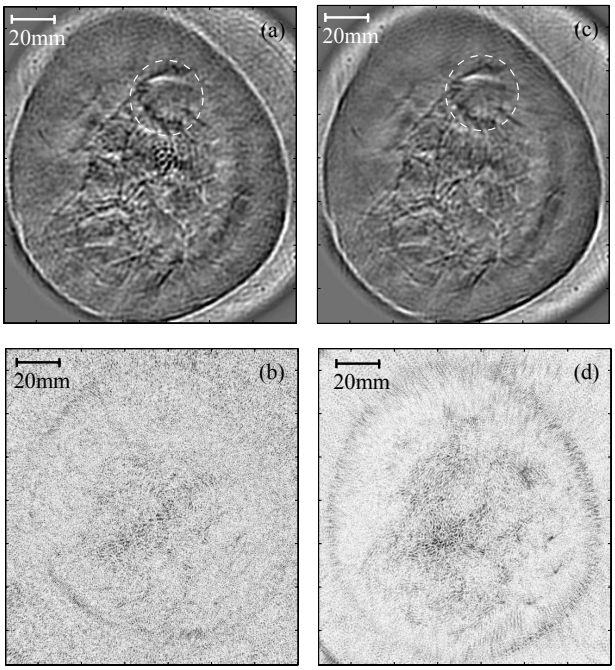

Figure 5. Images of a human breast *in vivo*. (a) and (b) CW transmission and RIs; (c) and (d) broadband transmission and RIs.

Figure 5(a) is a CW TDT of a coronal slice of the breast at 750kHz. The image shows the skin of the breast and a complex network of fibrous structures in the central part of the breast which could correspond to the ducts or Cooper's ligaments. The dashed circle indicates a region containing a tumor diagnosed with X-ray mammography and conventional ultrasound. Next, Fig. 5(b) is the coherent CW RI. This is biased by random noise and does not bear information about the breast anatomy. Figures 5(c) and (d) are coherent WB TDT and RI, respectively. Although the bandwidth was 100kHz only, a dramatic improvement can be observed in the case of the RI, Fig. 5(d), which now reveals the skin of the breast and some of the internal structures. On the other hand, little improvement is observed for the transmission image in Fig. 5(c) when compared to the CW image in Fig. 5(a).

5. CONCLUSIONS

This paper has investigated the use of wideband (WB) insonification in ultrasound tomography of human breast by means of experiments performed on two phantoms and a human breast *in vivo*. The study has compared continuous wave (CW) and WB insonifications and has considered both coherent and incoherent imaging methods.

The tests performed on a gel phantom with smoothly varying material properties have shown that transmission tomography is not sensitive to the frequency diversity of WB insonification. On the other hand, reflection tomography benefits from WB excitation since backscattering measurements have lower SNR than transmission measurements and the coherent combination of multiple CW images averages out the effect of random noise.

Experiments on a complex breast phantom, have shown that WB excitation can reduce the presence of speckle in incoherent imaging. However, incoherent imaging is sensitive to random noise that is amplified as different CW image are added incoherently.

These results have been confirmed by the *in vivo* experiments. In particular, they have shown that while transmission tomography has little sensitivity to frequency diversity, reflection tomography greatly benefits from WB excitation when the SNR is low.

Finally the experiments with the gel phantom and the breast *in vivo* suggest that reflection imaging is overall poorer than transmission tomography.

ACKNOWLEDGMENTS

This work was supported through the U. S. DOE Laboratory Directed Research and Development program at Los Alamos National Laboratory. FS is also grateful to the UK Royal Academy of Engineering / EPSRC for supporting this work. ND acknowledges the support of the Michigan Economic Development Corporation (MEDC) under grant MEDC 06-1-P1-0653.

REFERENCES

1. J. F. Greenleaf, S. A. Johnson, S. L. Lee, G. T. Herman, and E. H. Wood, "Algebraic reconstruction of spatial distributions of acoustic absorption within tissue from their two-dimensional acoustic projections," in *Acoustical Holography*, P. S. Green, ed., **5**, pp. 591–603, Plenum Press, New York, 1973.
2. J. F. Greenleaf, S. A. Johnson, W. F. Samayoa, and F. A. Duck, "Algebraic reconstruction of spatial distributions of acoustic velocities in tissue from their time-of-flight profiles," in *Acoustical Holography*, P. S. Green, ed., **6**, pp. 71–90, Plenum Press, New York, 1975.
3. P. L. Carson, C. R. Meyer, A. L. Scherzinger, and T. V. Oughton, "Breast imaging in coronal planes with simultaneous pulse echo and transmission ultrasound," *Science* **214**(4), pp. 1141–1143, 1981.
4. T. M. Kolb, J. Lichy, and J. H. Newhouse, "Comparison of the performance of screening mammography, physical examination, and breast us and evaluation of factors that influence them: An analysis of 27,825 patient eveluation," *Radiology* **225**, pp. 165–175, 2002.
5. M. P. Andre, M. P. Janee, H. S., G. P. Otto, B. A. Spivey, and P. D. A., "High-speed data acquisition in a diffraction tomography system employing large-scale toroidal arrays," *Int. J. Imag. Syst. Tech.* **8**, pp. 137–147, 1997.
6. F. Lin, A. I. Nachman, and R. C. Waag, "Quantitative imaging using a time-domain eigenfunction method," *J. Acoust. Soc. Am.* **108**(3), pp. 899–912, 2000.
7. R. C. Waag, F. Lin, T. K. Varslot, and J. P. Astheimer, "An eigenfunction method for reconstruction of large-scale and high-contrast objects," *IEEE Trans. Ultrason. Ferroelectr. Freq. Control* **54**(7), pp. 1316–1332, 2007.
8. N. Duric, L. Littrup, P. Poulo, A. Babkin, R. Pevzner, E. Holsapple, O. Rama, and C. Glide, "Detection of breast cancer with ultrasound tomography: First results with the computed ultrasound risk evaluation (cure) prototype," *Med. Phys.* **34**(2), pp. 773–785, 2007.
9. S. R. Deans, *The* R*adon transform and some of its applications*, Wiley, New York, 1983.
10. P. R. Williamson and M. H. Worthington, "Resolution limits in ray tomography due to wave behavior: Numerical experiments," *Geophysics* **58**(5), pp. 727–735, 1993.
11. E. Wolf, "Three-dimensional structure determination of semi-transparent objects from holographic data," *Opt. Commun.* **1**, pp. 153–156, 1969.
12. A. C. Kak and M. Slaney, *Principles of computerized tomographic reconstruction*, IEEE Press, New York, 1999.
13. J. G. Abbott and F. L. Thurstone, "Acoustic speckle: theory and experimental analysis," *Ultrason. Imag.* **1**, pp. 303–324, 1979.
14. J. G. Berryman, L. Borcea, G. C. Papanicolaou, and T. C., "Statistically stable ultrasonic imaging in random media," *J. Acoust. Soc. Am.* **112**(4), pp. 1509–1522, 2002.
15. M. Born and E. Wolf, *Principles of Optics*, Cambridge University Press, Cambridge, 1999.
16. F. Simonetti and Huang, "From beamforming to diffraction tomography," *J. Appl. Phys.* , p. Submitted, 2007.
17. F. Simonetti, L. Huang, N. Duric, and O. Rama, "Imaging beyond the born approximation: An experimental investigation with an ultrasonic ring array," *Phys. Rev. E* **76**, p. 036601, 2007.
18. F. Simonetti, L. Huang, and N. Duric, "High-resolution ultrasound tomography of complex three-dimensional objects," *submitted for publication* , 2007.